Bio-mimetic Impedance Control of Robotic Manipulator for Dynamic Contact Tasks

Toshio Tsuji, and Yoshiyuki Tanaka

1-4-1, Kagamiyama, Higashi-Hiroshima, 739-8527 JAPAN, Department of Artificial Complex Systems Engineering, Graduate school of Engineering, Hiroshima University

Abstract

A human performs a variety of skillful movements by adjusting dynamic characteristics of his or her musculoskeletal system according to a task involved. Such characteristics of human movements can be described by mechanical impedance parameters. If the regulation mechanism of human impedance properties during the task can be clarified and modeled, there is a possibility that human skillful strategies can be integrated into robot motion control. This paper investigates human hand impedance in preparation for task operations, so-called "*task-readiness impedance*," in a virtual ball-catching task. It further discusses a biomimetic impedance control of robotic manipulators for contact tasks via computer simulations using measured task-readiness impedance.

Key words: Human arm movements, impedance control, contact tasks, robotic manipulator

1 Introduction

A human performs a variety of skillful movements by adjusting dynamic characteristics of his musculoskeletal system according to a task involved. In a ball-catching task, for instance, a human player might miss a ball when he stiffens his arm beyond necessity for catching the ball due to large contact force exerted by the hand on the ball. When the player's arm is too compliant, however, he also might miss because he cannot generate enough hand force to absorb the ball's motion. Thus, the player has to regulate the mechanical properties of his arm to catch a ball according to the task conditions, such as ball speed, weight, and size. In general, such dynamic characteristics of a human hand can be described using mechanical impedance parameters: stiffness, viscosity, and inertia. If the regulation mechanism of human impedance

properties during tasks can be clarified and modeled, we should be able to integrate these skillful human strategies into robot motion control. The final goal of this study is to develop a biomimetic impedance control for robots to perform contact tasks by using human impedance parameters.

Much research has been done on robot motion programming to perform tasks on the basis of human demonstrations, in which a mathematical model of skillful human movements for maneuvering a robotic tool is expressed in terms of mechanical impedance. Liu and Asada [1] pioneered this research area, and many other studies have followed their work [2]-[6]. Although these previous studies described the characteristics of human movements in the framework of an impedance model, they did not investigate human impedance properties involved in tasks.

Many experimental studies on human hand impedance have reported on multi-joint arm movements. For example, Mussa-Ivaldi, et al. [7] pioneered the measurement of human hand impedance, and examined hand stiffness in a stable arm posture. They found that hand stiffness strongly depends on arm posture, and that a human can change the size of a stiffness ellipse although he can change neither the orientation nor the shape of it. Dolan et al. [8] and Tsuji et al. [9], [10] investigated not only hand stiffness but also viscosity and inertia, and verified a qualitative analogy between hand stiffness and viscosity. Tsuji, et al. [11] also showed that the human hand's viscoelasticity changes radically with respect to the muscle activation level during isometric contraction in the upper limb. Gomi and Kawato [12] estimated hand stiffness during reaching movements, reporting that the stiffness changes considerably during reaching movements in comparison with that in a stable arm posture. They also calculated the virtual trajectory using estimated hand impedance parameters. These studies, however, do not discuss the adaptation mechanism of human impedance depending on task conditions, and the arm movements were restricted to the horizontal plane.

Unlike the studies above, Bennett et al. [14] described the dynamic properties of human movements using an open-loop transfer function, and analyzed the gain and phase characteristics of catching a falling ball through experiment results with human subjects. They examined the change of transfer characteristics caused by stretch reflex and voluntary muscle activation under various catching conditions. Their research focused on hand impedance in the uniarticular movements of the elbow joint, not multi-joint arm movements. The regulation of human hand impedance, however, was not resolved even though the target task is a dynamic movement. Lacquanti et al. [15] examined the time-varying changes in human hand impedance parameters during a catching task, in which arm movements were restricted to the vertical plane and a ball was dropped into the hand of a human subject. Hand viscoelastic properties were computed from angular ones of the elbow and wrist joints estimated

by applying continuous pseudorandom perturbations at the elbow joint while inertia computed from the moment of inertia with a two-joint arm model. They showed that a human actively changes his/her hand viscoelastic properties around impact time during catching a falling ball, and suggested the existence of a parallel neural control of hand impedance parameters. However, hand viscoelastic properties were estimated under the strict condition that the timing of the impact was fixed relative to a sequence of the perturbations in every trial because the designed task was a passive one, and the influence of environmental dynamics, such as weight and speed of a ball, onto human arm movements was not discussed.

This paper investigates the regulation mechanism of human hand impedance in multi-joint arm movements during a virtual ball-catching task according to environmental dynamics, and aims to develop a bio-mimetic motor control strategy of a robotic manipulator for dynamic contact tasks in the framework of a robot impedance control method [16]. The present paper is organized as follows: Section 2 describes an estimation method of task-readiness impedance for dynamic tasks based on the virtual-trajectory control hypothesis. Section 3 explains the experimental system using a robotic device developed for a virtual ball-catching task and the experimental procedure for analyzing the changes in hand impedance properties during the task. In Section 4, the regulatory ability of human hand impedance during the task according to experimental conditions is analyzed by associating with hand movements and arm posture from a set of experimental results. Then, the potentiality of a bio-mimetic impedance control is verified through computer simulations using estimated human hand impedance and virtual trajectory.

2 Task-Readiness Impedance

2.1 Method of Impedance Measurement

Let us consider multi-joint movements of the human upper extremity in the l-dimensional task space. When an end-point of a subject is displaced from its equilibrium by a small disturbance with a short duration as shown in Fig. 1, the dynamic characteristics of the hand can be expressed with an impedance model [9], [10] as

$$M_e\ddot{X}_e(t) + B_e\dot{X}_e(t) + K_e(X_e(t) - X_v(t)) = -F_e(t), \tag{1}$$

where $F_e(t) \in \Re^l$ is the hand force applied to the environment; $X_e(t) \in \Re^l$ the hand position; $X_v(t) \in \Re^l$ the virtual trajectory; and M_e, B_e, and $K_e \in \Re^{l\times l}$

are hand inertia, viscosity and stiffness, respectively. Assuming that the virtual trajectory $X_v(t)$ does not change during the external disturbance of short duration induced for measuring human impedance during stable arm posture, the following equation of hand dynamics can be derived from (1):

$$M_e d\ddot{X}(t) + B_e d\dot{X}(t) + K_e dX(t) = -dF_e(t), \tag{2}$$

where $dX(t) = X_e(t) - X_e(t_0)$, $dF(t) = F_e(t) - F_e(t_0)$, and t_0 is the time when the disturbance is applied to the hand. In this model, the hand impedance matrices can be estimated from the measured hand position $X_e(t)$ and the hand force $F_e(t)$ from the least-squares method [10].

In dynamic tasks, however, $X_v(t)$ usually changes, and the only measurable variables are hand position $(X_e(t), \dot{X}_e(t), \ddot{X}_e(t))$ and hand force $(F_e(t))$. Therefore, M_e, B_e, K_e, and $X_v(t)$ cannot be uniquely determined from (2). Besides, hand impedance should be regarded as a time-varying factor since the impedance parameters change according to the arm posture and the muscle contraction level during dynamic tasks [12]. It is thus very difficult to estimate hand impedance during dynamic tasks.

On the other hand, a human needs to regulate his hand impedance before motion for some target tasks. In the ball-catching task, for instance, a player should adjust his hand impedance before catching a ball according to the motion and physical properties of the approaching ball, otherwise it would be too late to prepare for the task. This suggests that the skilled player must successfully perform such a task by adjusting his hand impedance to the desired properties in preparation for the motion on the basis of his prior experience. Accordingly, the hand impedance parameters can be estimated using (2) since the virtual trajectory, $X_v(t)$, does not much change in the preliminary phase before motion.

This paper focuses on such hand impedance in that preliminary phase, the so-called *task-readiness impedance*. Although task-readiness impedance differs from human impedance in dynamic motion, a human regulates his task-readiness impedance according to a task before any motion occurs. Thus, analyzing task-readiness impedance may clarify a neurological function of human impedance regulation, such as learning ability and the adaptation mechanism of human impedance properties according to tasks.

2.2 Virtual Trajectory

In the virtual-trajectory control hypothesis [13], hand motion is created by the changes of the virtual trajectory, and the interaction force with environ-

ments as well as the hand impedance properties during a task. Therefore, if the interaction force to the hand were suddenly removed in a well-practiced motion, the hand would attempt to follow the virtual trajectory acquired from experiences.

Applying this hypothesis to the ball-catching task, for instance, such phenomena can be observed when a ball is unexpectedly disappeared just before a player is catching the ball as shown in Fig. 2, in which he cannot feel any interaction force. At this situation, the virtual trajectory can be calculated from (1) as follows:

$$X_v(t) = K_e^{-1}(F_e(t) + M_e\ddot{X}_e(t) + B_e\dot{X}_e(t)) + X_e(t), \tag{3}$$

where M_e, B_e, and K_e denote the task-readiness impedance parameters.

The virtual trajectory calculated by (3) represents hand movements until just after motion. Although the hand impedance may start changing just before motion, the difference between the task-readiness impedance and the hand impedance just after motion is so small that the virtual trajectory derived by (3) is almost equal to the true virtual trajectory just after the motion begins.

Consequently, we estimate the task-readiness impedance and the virtual trajectory by providing the enforced displacement needed to move the hand in the missed-catch operation. However, it is not easy to implement such an instantaneous operation during a real ball-catching task in the multi-dimentional task space. Since the virtual-trajectory control hypothesis stands up in the one-dimentional task space, a virtual ball-catching task requiring straight hand motion is therefore demonstrated in the virtual space by using virtual reality technology in this paper.

3 Virtual Ball-Catching Task

3.1 Experimental Apparatus

Figure 3 depicts the experimental apparatus developed in this study. The system is composed of a robot that provides the interaction force generated between the virtual ball and the racket, a computer for robot motion control as well as signal processing, and a display to show the task information to a human subject. A subject is required to hit the virtual ball by operating the handle attached to the robot with the visual information provided on the bio-feedback display, while the robot presents the interaction force to the subject in hitting the ball.

The robot is constructed with a linear motor table (Nippon Thompson Co., Ltd.; maximum driving force 10 [kgf]; stroke length 400 [mm]; encoder resolution 2 [μm]), which is impedance-controlled so the virtual interaction force between the virtual ball and the racket handle can be displayed to the subject. A six-axis force sensor (B.L. Autotech Co., Ltd.; resolution: translational force on x- and y-axes 5×10^{-3} [N], on z-axis 15×10^{-2} [N], torque 3×10^{-3} [Nm]) is attached at the base of the handle to measure the operating force of the subject.

Figure 4 illustrates the accuracy of estimated impedance parameters with a known spring-mass system in the prototype system, where mean values for five sets of the estimated results are plotted. We attached a weight to the racket handle of the robot, setting a spring between the handle and the fixed environment. The intersections of the dotted lines in the figure represent the true values of impedance parameters set at the robot handle. Both stiffness and inertia estimates were almost correct, where the standard deviations for estimated stiffness and inertia were less than 4.53 [N/m] and 0.01 [kg].

A human can change hand impedance properties by adjusting a muscle-contraction level as well as arm posture [11]. To investigate a mechanism of human impedance regulation, we measured the surface EMG signals from the wrist joint flexor (flexor carpi radialis: FCR) and extensor (extensor ulnaris: ECU), the elbow joint flexor (biceps brachii: BB) and extensor (triceps brachii: TB), and the shoulder joint flexors (pectoralis major: PM, deltoideus anterior: DA) and extensors (teres major: TM, deltoideus posterior: DP). The sampling rate for measuring hand movements and EMG signals was set at 1 [kHz] in the experiments. We also used a stereo video camera system with two CCD cameras (Quick MAG: Oh-yoh Keisoku Kenkyusho, sampling rate: 60 [Hz]) to observe the subject's arm posture shown by the detected three-dimensional positions of color markers attached to the subject's body. In this paper, a human body is represented by a rigid-link model with 11 rotational joints, as shown in Fig. 5.

A set of experiments were carried out with four male subjects (22 - 24 of year, all right-handed) in this paper. The measurement time in each trial was set at $t_e = 5$ [s] and the sampling time at $\Delta t = 1$ [ms].

3.2 A Model of Virtual Ball-catching Task

Figure 6(a) presents an overview of a virtual ball-catching task in a one-dimensional task space ($l = 1$) in which the ball is hung from the ceiling at X_f by a rigid pendulum with length L and angle θ. The initial position of the hand is set at the origin of the task space. The virtual ball is approximated

with a viscoelastic model as shown in Fig. 6(b), and the racket is regarded as a rigid body.

The interaction force F_{int} between the ball and the racket is calculated from the relative position $X_r(t)(= X_o(t) - X_e(t))$ by

$$F_{int}(t) = \begin{cases} B_b d\dot{X}_b(t) + K_b dX_b(t) & (|X_r(t)| \leq R_b) \\ 0 & (|X_r(t)| > R_b) \end{cases}, \tag{4}$$

$$dX_b(t) = X_r(t) - R_b n, \tag{5}$$

$$n = \begin{cases} \dfrac{X_r(t)}{|X_r(t)|} & (X_r(t) \neq 0) \\ 0 & (X_r(t) = 0) \end{cases}, \tag{6}$$

where B_b and K_b are the viscoelastic properties of a ball with weight M_b and radius R_b; and $dX_b(= X_r - R_b n)$ represents a dent in the ball produced by contact with the racket.

The robotic table is under impedance control [16] so that the racket position $X_e(t)$ follows

$$M_r \ddot{X}_e(t) + B_r \dot{X}_e(t) = F_{int}(t) + F_e(t), \tag{7}$$

where M_r, and B_r denote the desired inertia and viscosity of the robot. Fig. 7 (a) illustrates a block diagram of the impedance-controlled robot, where F_{act} expresses a control input to the robot. Modeling the system dynamics of a real robot, $R(s)$, by

$$R(s) = \frac{1}{Ms^2 + Bs}, \tag{8}$$

the impedance control is expressed as shown in Fig. 7 (b), where M and B are inertia and viscosity. The employed robot in this paper has $M = 4.7$ [kg] and $B = 47$ [Ns/m].

3.3 Experimental Procedure

A subject is asked to perform a ball-catching task 120 times continuously, in which the following five operations are executed in random order to measure

human-hand impedance: (I) measurement of hand impedance while maintaining stable arm posture; (II) measurement during the stable phase before motion; (III) measurement of task-readiness impedance in the preliminary phase; (IV) measurement of hand impedance after motion; and (V) estimation of the virtual trajectory when the ball is suddenly disappeared just before contacting with the racket so that a subject could not strike the ball and feel any interaction force unexpectedly. This missed-catch operation was artificially conducted during repeated trials. The subject is then instructed to maintain his arm postures until just before motion.

In the target task, a subject is required to control his arm movements so that the interaction force between the virtual ball and the racket becomes small as much as possible at the impact time, otherwise the ball would rebound from the racket. Therefore, the skill level of subjects for the target task is evaluated by the maximum interaction force between the ball and the racket, F_{int}^{max}, and the period of the time during the ball contacts with the racket, t_{int}, defined by

$$F_{int}^{max} = \max_{0 \le t \le t_e} F_{int}(t), \tag{9}$$

$$t_{int} = \sum_{t=0}^{t_e} u(t)\Delta t, \tag{10}$$

where

$$u(t) = \begin{cases} 1 \ (F_{int}(t) \neq 0) \\ 0 \ (F_{int}(t) = 0). \end{cases} \tag{11}$$

Namely, it is regarded that the skill level of the subject for the task is better as the value of F_{int}^{max} is smaller while the value of t_{int} is larger.

Figures 8 and 9 present examples of experiment results for an unskilled Subject A and a skilled Subject C during the ball-catching task, in which no external disturbance is induced to estimate hand impedance parameters. The solid lines in the figure (a) represent the hand position of each subject while the dotted lines are the ball position. The figure (b) illustrates the time profile of the subject's hand force during the catching task. The skilled subject completes the target task with smooth hand movements by adjusting his hand velocity according to the ball motion, while the unskilled subject did not catch the ball, which rebounded off the racket as shown in Fig. 8. It can be observed that the hand force applied by Subject A is much less than that applied by Subject C.

Table 1 shows the mean values of F_{int}^{max} and t_{int} with standard deviations for

a set of 120 trials by the subjects. Subjects C and D generated less hand force for catching the ball with a longer contact period than Subjects A and B. These results indicate that Subjects C and D have better skill in the target task than Subjects A and B.

Figure 10 shows an example of EMG signals of the skilled Subject C performing the task for five seconds, measured from one second before a starting signal appeared on the display, and in which the racket contacted the ball at $t_c = 2.6$ [s]. The figure shows that the subject contracted his arm muscles to prepare for the target task before the racket contacted the ball.

Since the subject began to activate his arm muscle from $t = 2.5$ [s], the external disturbances to the subject's hand for Operations I, II, III, and IV were induced at $t_0 = 0$, 0.5, 2.3 (about 0.3 [s] before the contact), and 4.5 [s], respectively. Shaded zones in Figs. 8, 9 and 10 express the measuring terms for estimating hand impedance parameters in each of the operations.

4 Experimental Results

4.1 Human Hand Impedance During the Task

Figure 11 illustrates an example of hand movements measured in Operation IV for estimating task-readiness impedance. The figures (a), (b), and (c) express the time history of hand position $X_e(t)$, hand velocity $\dot{X}_e(t)$, and hand acceleration $\ddot{X}_e(t)$ caused by the external disturbance from the top. The solid line in Fig. 11 (d) represents the measured hand force together with the estimated hand force (the dotted line) calculated from (2), with the measured hand movements and the estimated hand-impedance parameters (K_e, B_e, and M_e). Fig. 11 (d) demonstrates that the model in (2) can accurately describe the dynamic characteristics of human movements because the solid line almost coincides with the dotted one.

Table 2 lists the mean values of the estimated impedance for each of five operations with standard deviations and the correlation coefficients ρ between the measured and the estimated hand force by using the least squares method with (2). Hand impedance was estimated with the same posture during Operations I $\sim$ III. Tables (a), (b), (c), and (d) describe the impedance properties in Operations I, II, III, and IV, respectively. Asterisks, ***, and *** refer to the estimated impedance parameters with statistical differences at significance levels of 5, 3, and 1% for hand-impedance parameters in the stable-arm posture determined by the one-sided t-test.

It is obvious from the experimental results that all subjects increase hand stiffness estimated before motion (Operation II) compared with one in maintaining a stable arm posture before motion (Operation I). Consequently, it can be said that a human regulates his hand impedance properties before starting motions for a task. On the other hand, there are not significant differences between the estimated hand impedance in Operations II and III, except for Subject C. This result strongly suggests that a human had already begun regulating his hand impedance quite before starting motions. It can be also seen from Fig. 10 because the subjects contracted each muscle in the upper extremities from the beginning of the task ($t = 0$ [s]). Note that Subject C had already contracted his muscle from about 1.5 [s] so that his task-readiness stiffness was larger than that estimated before motion.

The task-readiness impedance parameters of the skilled subjects are greater than those of the unskilled subjects as shown in Table 2 (c). To explain this difference dependent on human skill levels, we examined the arm movements from the change of joint angles. Fig. 12 shows the examples of arm postures during the task measured by a stereo camera system. The skilled subject raised the elbow joint higher than the unskilled subject during the task, and tried to utilize the whole arm to carry out the ball-catching task. This indicates that the skilled subject increased his hand inertia to suppress the effect of the contact force exerted by the ball. Fig. 13 represents the time profiles in the catching movement of the shoulder joint angle θ_5 (the solid line), the elbow joint angle θ_8 (the broken line), and the wrist joint angle θ_{11} (the dotted line). The skilled subject actively changed his joint angles for a short time before contacting the ball so his hand velocity would be the same as the ball velocity.

Table 3 shows the damping coefficients and the natural frequencies of the hand motion during Operation III that calculated from the estimated task-readiness impedance in Table 2 (c). It can be seen that the damping coefficients of the skilled subjects are less than those of the unskilled subjects while the natural frequencies are greater. This result indicates that the skilled subjects decreased the damping of the hand movements while adjusting the hand's viscoelastic properties to improve the tracking performance of the hand for virtual trajectory.

We also calculated the virtual trajectory with the estimated task-readiness impedance. Figs. 14 and 15 show the experimental results in Operation V for the skilled and unskilled subjects. The figure (a) shows the time history of the hand position (the solid lines) and the ball position (the dotted lines), (b) shows the hand force during the task, and (c) shows the virtual trajectory (the solid lines) and the hand position (the dotted lines). The time t_c is the time when the racket contacts the ball. Regardless of the skill levels of the subjects, they greatly changed the virtual trajectory to adjust the velocity of the hand to the ball's motion so the hand velocity would be maximized at the contact.

Although there are not remarkable differences in the virtual trajectories just after the contact for either skill level, the natural frequency of the skilled subject's end-point was greater than that of the unskilled subject. (See Table 3.) The skilled subject increased the response of hand mobility to better follow the virtual trajectory.

4.2 Changes in Human Hand Impedance Depending on Task Conditions

The above results strongly suggest that the subjects performed the target task by regulating both task-readiness impedance and virtual trajectory at the same time, according to the task conditions. We conducted further experiments by changing robot viscosity from $B_r = 20$ [Ns/m] to $B_r = 5$ [Ns/m], and examined how the skilled Subjects C and D adjusted task-readiness impedance depending on the dynamic properties of the task environment.

Figure 16 presents examples of experimental results for $B_r = 5$ [Ns/m], where the solid and dotted lines represent the hand position of each subject and the position of the ball during the task. Subject C carried out the catching task smoothly, while Subject D bounced the ball on the second contact since he did not suppress the ball motion completely at the first contact.

Table 4 presents the mean values with standard deviations of F_{int}^{max} and t_{int} for 120 measurements with $B_r = 5$ [Ns/m]. The values of F_{int}^{max} and t_{int} by Subject D were less than those by Subject C, although they had almost the same score for $B_r = 20$ [Ns/m] (See Table 1). According to Fig. 16 and Table 4, Subject D needed a longer time to reach the equilibrium for catching a ball than Subject C did.

Table 5 lists the mean values with standard deviations of the estimated task-readiness impedance. Subject C increased his hand viscosity, as well as hand stiffness, more than for $B_r = 20$ [Ns/m], to compensate for the decrease of racket viscosity (See Table 2 (c)), so the dynamic characteristics of the whole system including the human hand and the robot are almost equal in the case of $B_r = 20$ [Ns/m]. For Subject D, the whole system became less damped, since he increased mainly hand stiffness. As a result, Subject D did not perform the ball-catching task as well as Subject C.

These experimental results demonstrate that a human adaptively changes task-readiness impedance as well as virtual trajectory during tasks depending on task conditions.

Finally, computer simulations are conducted to reproduce human hand movements in the ball-catching task using estimated task-readiness impedance and virtual trajectory, assuming that the dynamic characteristics of the human hand follow the impedance model given in (1).

Figure 17 depicts the simulated result with the estimated task-readiness impedance of the unskilled Subject A, which corresponds to the experimental result in Fig. 8. Similarly, Fig. 18 presents the simulated result using the task-readiness impedance of the skilled Subject C, which corresponds to Fig. 9. The solid line in Fig. 18(a) represents the time profiles for the hand position; the dotted line represents the time profiles for the ball position; and the solid line in Fig. 18(b) represents the virtual hand trajectory.

The momentum of the virtual ball in Fig. 18 was absorbed successfully and the ball advanced smoothly to an equilibrium point for catching, while the ball in Fig. 17 bounced off the hand. These results show that the task-readiness impedance and the estimated virtual trajectory properly express the dynamic properties of human movements during task performance.

The proposed methodology with a human impedance model has potential for describing human skills and strategies for a task, which will be a key factor for developing a human-like robot.

5 Conclusion

This paper discussed how a human regulates his hand impedance properties for dynamic-contact tasks and analyzed the task-readiness impedance and the virtual trajectory of the hand in a virtual ball-catching task. From a set of the experimental and simulated results, we defined the following points on human movements:

- Human strategies for tasks can be modeled using mechanical impedance properties.
- Human impedance properties can be utilized to describe the skill level for tasks performed by a human.
- A human regulates his impedance properties appropriately during target tasks.

Future research will investigate task-readiness impedance according to impedance properties of an object and a robot, and the influence of bio-feedback in-

formation during task performance in detail. We will also plan to examine task-readiness impedance during another task in the multi-dimentional virtual space.

Acknowledgments

The authors would like to thank Prof. M.Kaneko of Hiroshima University for his helpful comments and discussions. This research work was supported in part by a Grant-in-Aid for Scientific Research from the Japanese Ministry of Education, Science and Culture (15360226 and 16760203).

References

[1] S. Liu and H. Asada: "Transferring Manipulative Skills to Robot: Representation and Acquisition of Tool Manipulative Skills Using a Process Dynamics Model," *Transactions of the ASME, Journal of Dynamic System, Measurement and Control*, vol. 114, no. 2, pp. 220–228, 1992.

[2] P. Sikka and B. J. McCarragher: "Stiffness-based Understanding and Modeling of Contact Tasks by Human Demonstration," in Proceedings of *the IEEE/RSJ International Conference on Intelligent Robots and Systems*, pp. 464–470, 1997.

[3] J. E. Colgate: "Robust Impedance Shaping Telemanipulation," *IEEE Transactions on Robotics and Automation*, vol. 19, no. 4, pp. 374–384, 1993.

[4] K. Kosuge, Y. Fujisawa, and T. Fukuda: "Control of Mechanical System with Man-machine Interaction," in Proceedings of *the IEEE/RSJ International Conference on Intelligent Robots and Systems*, pp. 87–92, 1992.

[5] O. M. Al-Jarrah and Y. F. Zheng: "Arm-manipulator coordination for load sharing using compliant control," in Proceedings of *the IEEE International Conference on Robotics and Automation*, pp. 1000–1005, 1996.

[6] R. Ikeura: "Manual Control Approach to the Teaching of a Robot Task," *IEEE Transaction on Systems, Man and Cybernetics*, vol. 24, no. 9, pp. 1339–1346, 1994.

[7] F. A. Mussa-Ivaldi, N. Hogan, and E. Bizzi: "Neural, Mechanical and Geometric Factors Subserving Arm in Humans," *Journal of Neuroscience*, vol.5, no. 10, pp. 2732–2743, 1985.

[8] J. M. Dolan, M. B. Friendman, and M. L. Nagarka: "Dynamics and Loaded Impedance Components in The Maintenance of Human Arm Posture," *IEEE Transaction on Systems, Man, and Cybernetics*, vol.23, no. 3, pp. 698–709, 1993.

[9] T. Tsuji, K. Goto, K. Ito and M. Nagamachi: "Estimation of Human Hand Impedance During Maintenance of Posture," *Transactions of the Society of Instrument and Control Engineers*, vol. 30, no. 3, pp. 319–328, 1994. (in Japanese)

[10] T. Tsuji, P. G. Morasso, K. Goto, and K. Ito: "Human Hand Impedance Characteristics during Maintained Posture," *Biological Cybernetics*, vol. 72, pp. 457–485, 1995.

[11] T. Tsuji, M. Moritani, M. Kaneko and K. Ito: "An Analysis of Human Hand Impedance Characteristics : During Isometric Muscle Contractions," *Transaction of the Society of Instrument and Control Engineers*, vol. 32, no. 2, pp. 271–280, 1996. (in Japanese)

[12] H. Gomi, and M. Kawato: "Human Arm Stiffness and Equilibrium-point Trajectory during Multi-joint Movement," *Biological Cybernetics*, vol. 76, pp. 163–171, 1997.

[13] N. Hogan: "The Mechanics of Multi-Joint Posture and Movement Control," *Biological Cybernetics*, vo. 52, pp. 315–331, 1985.

[14] D. J. Bennett, M. Gorassini, and A. Prochazka: "Catching a Ball: Contributions of Intrinsic Muscle Stiffness, Reflexes, and Higher Order Responses," *CAN. J. PHYSIOL. PHARMACOL*, vol. 72, pp. 525–534, 1994.

[15] F. Lacquanti, M. Carrozzo, and N. A. Borghess: "Time-varying Mechanical Behavior of Multijointed Arm in Man," *J. of Neurophusiology*, vol. 69, NO. 5, pp. 1443–1464, May 1993.

[16] N. Hogan: "Impedance Control: An Approach to Manipulation, Parts I, II, III," *Transactions of the ASME, Journal of Dynamic Systems, Measurement and Control*, Vol.107, No.1, pp.1–24, 1985.

List of Tables

Table 1
The maximum value of interaction force and contacting time of the subjects

		F_{int}^{max} [N]	t_{int} [s]
Subjects	A	32.91±3.15	1.16±0.45
	B	32.39±3.89	1.75±0.24
	C	25.15±6.83	1.70±0.29
	D	25.22±3.83	1.73±0.30

Table 2
Measured human hand impedance during the ball-catching task

(a) During maintenance of the stable posture

		K_e [N/m]	B_e [Ns/m]	M_e [kg]	ρ
Subjects	A	61.24±35.80	21.84±0.53	1.12±0.10	0.95±0.01
	B	43.69±23.71	12.37±1.66	0.94±0.06	0.92±0.01
	C	64.90±33.18	25.39±2.51	1.74±0.10	0.96±0.01
	D	98.34±45.04	22.65±3.53	1.64±0.11	0.93±0.02

(b) Before motion

		K_e [N/m]	B_e [Ns/m]	M_e [kg]	ρ
Subjects	A	72.74±42.51	25.22±2.29***	1.18±0.09	0.97±0.01
	B	85.78±47.10***	16.50±2.29***	1.00±0.11	0.97±0.01
	C	84.21±41.12	29.34±4.36*	1.74±0.12	0.96±0.01
	D	165.35±81.41**	21.04±4.37	1.71±0.18	0.96±0.01

(c) Task-readiness

		K_e [N/m]	B_e [Ns/m]	M_e [kg]	ρ
Subjects	A	61.47±30.42	24.26±3.12**	1.25±0.14*	0.98±0.01
	B	57.45±35.39	17.56±3.02***	0.83±0.17**	0.96±0.01
	C	188.89±71.20***	28.07±2.37*	1.90±0.16**	0.98±0.01
	D	154.81±103.40	22.27±2.95	1.76±0.23	0.96±0.01

(d) After motion

		K_e [N/m]	B_e [Ns/m]	M_e [kg]	ρ
Subjects	A	117.27±67.62**	24.98±3.42***	1.14±0.11	0.99±0.01
	B	82.02±43.70***	8.76±1.49***	0.81±0.10***	0.97±0.01
	C	97.97±57.05	23.94±4.53	1.44±0.18***	0.97±0.01
	D	156.17±103.89	10.04±2.88***	1.33±0.14***	0.98±0.01

*・・・5%　**・・・3%　***・・・1%

Table 3
Damping coefficients and natural frequencies of the subjects

		ζ	ω_n [rad/s]
Subjects	A	1.54 ± 0.46	6.81 ± 1.45
	B	1.65 ± 0.83	7.80 ± 1.90
	C	0.79 ± 0.22	9.79 ± 1.62
	D	0.84 ± 0.37	8.72 ± 2.70

Table 4
The maximum value of the interaction force and contacting time of the subjects for $B_r = 5$ [Ns/m]

		F_{int}^{max} [N]	t_{int} [s]
Subjects	C	25.96±4.45	1.73±0.26
	D	23.66±4.27	1.07±0.36

Table 5
Estimated task-readiness impedance for $B_r = 5$ [Ns/m]

		K_e [N/m]	B_e [Ns/m]	M_e [kg]	ρ
Subjects	C	128.83±74.76	37.21±4.65	1.74±0.15	0.98±0.01
	D	195.02±114.98	18.26±2.81	1.67±0.17	0.98±0.01

List of Figures

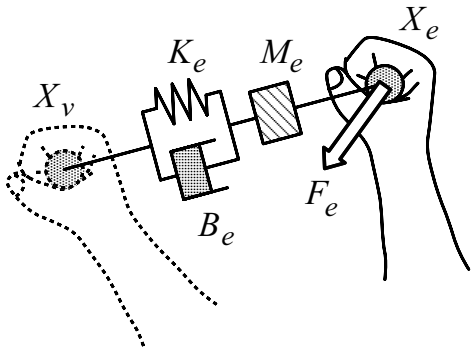

Fig. 1. Experimental apparatus for measuring task-readiness impedance in the virtual task

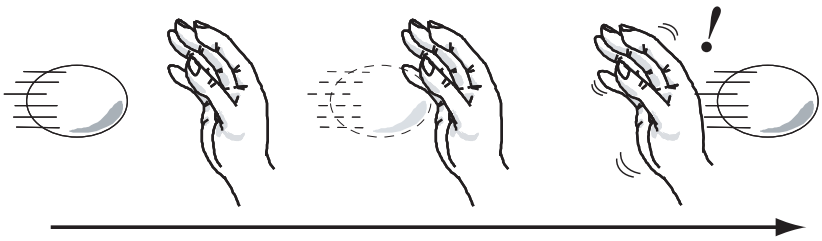

Fig. 2. Virtual trajectory control at an unexpected missing trial in the ball-catching task

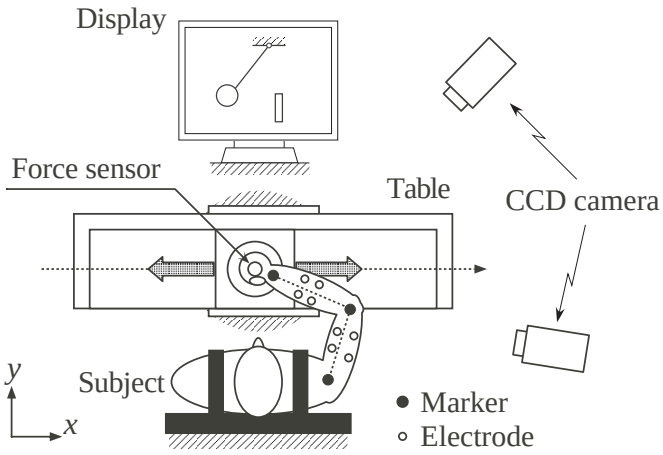

Fig. 3. Experimental apparatus for measuring task-readiness impedance in the virtual task

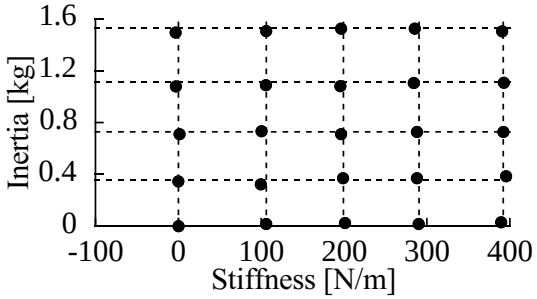

Fig. 4. Accuracy of estimated impedance estimated with a known spring-mass system in the developed prototype system.

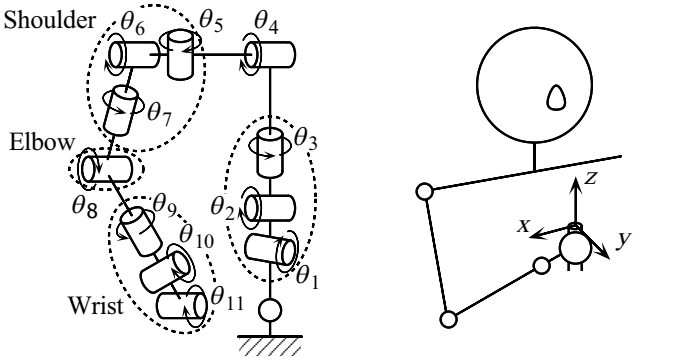

(a) Joint degrees of freedom of human arm

(b) Task coordinate system

Fig. 5. A link model of a human right-upper body

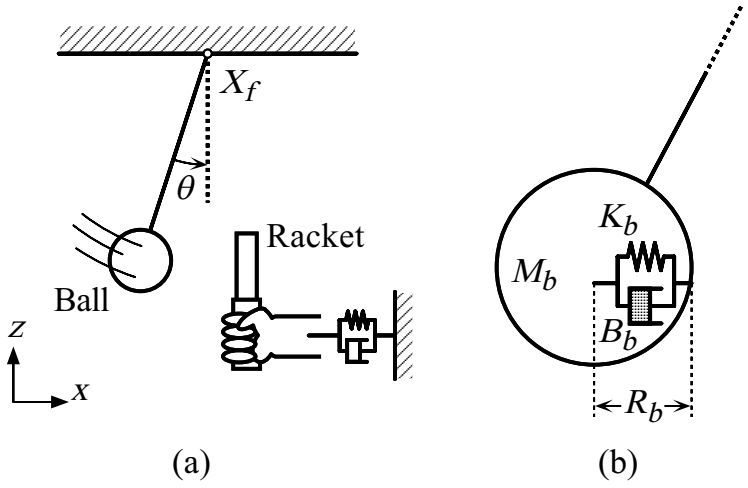

Fig. 6. A model of the virtual ball-catching task

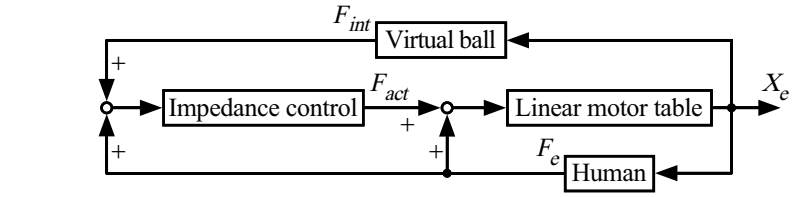

(a)

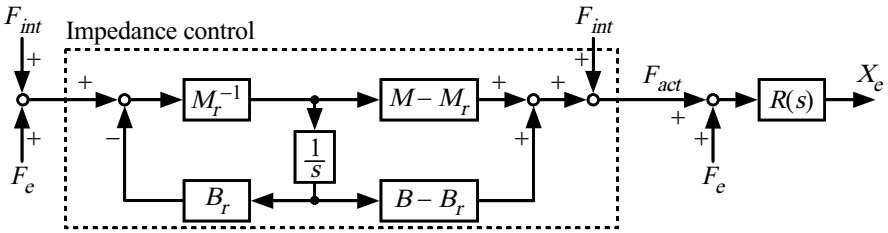

(b)

Fig. 7. Impedance control system for the ball-catching task

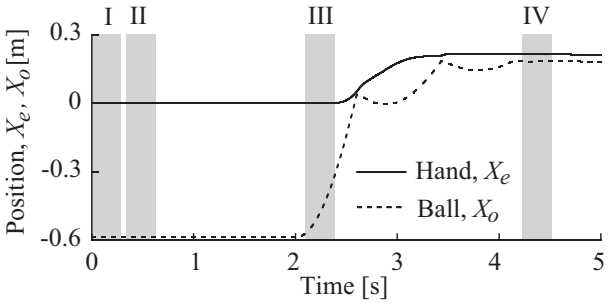

(a) Hand and ball positions

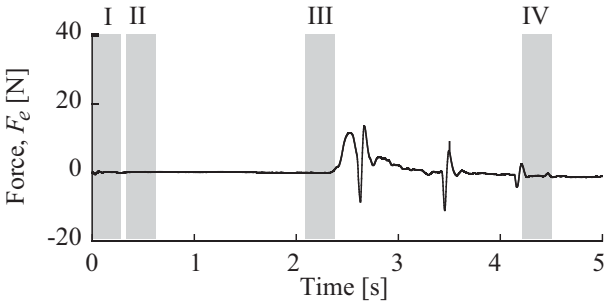

(b) Hand force

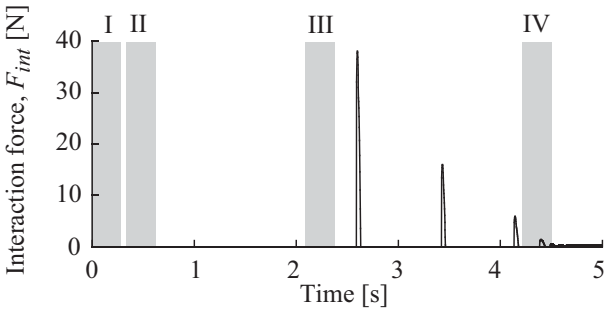

(c) Interaction force

Fig. 8. An example of experimental results of the unskilled subject A ($F_{int}^{max} = 38.09$ [N], $t_{int} = 0.69$ [s])

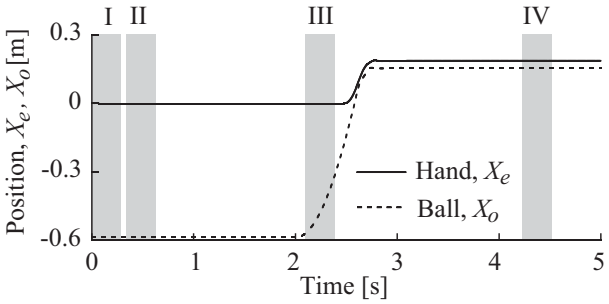

(a) Hand and ball positions

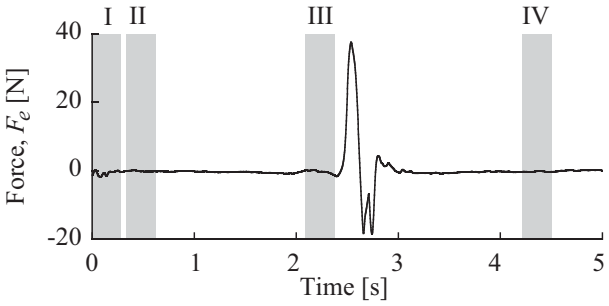

(b) Hand force

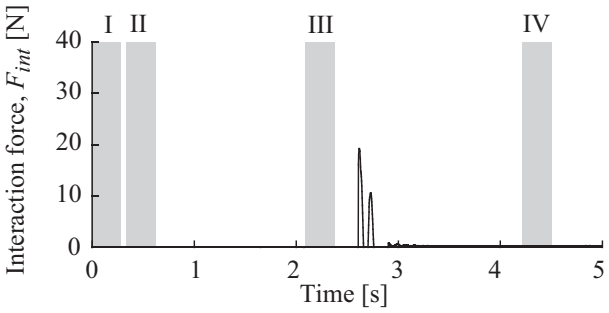

(c) Interaction force

Fig. 9. An example of experimental results of the skilled subject C ($F_{int}^{max} = 19.25$ [N], $t_{int} = 2.20$ [s])

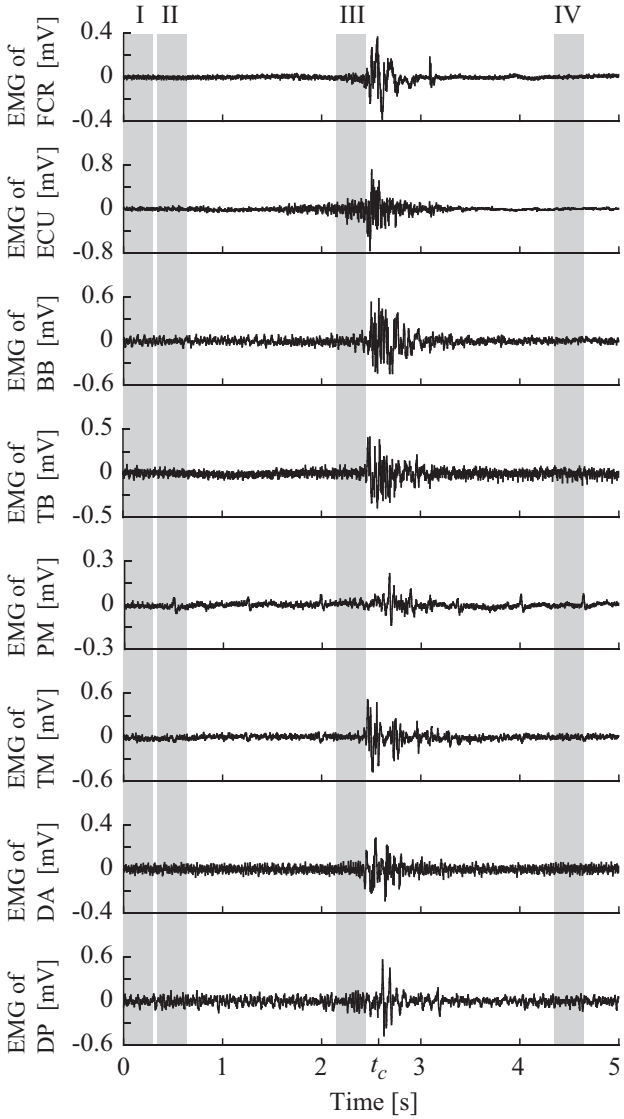

Fig. 10. An example of the measured EMG signals (Subject C)

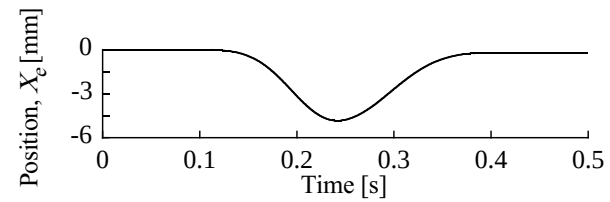

(a) Hand position

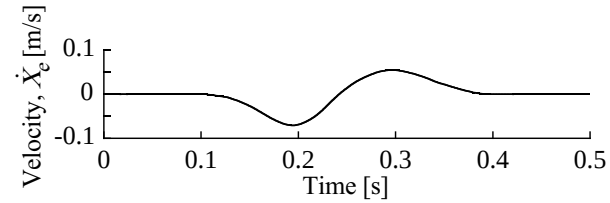

(b) Hand velocity

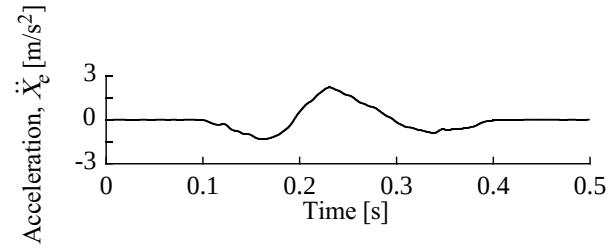

(c) Hand acceleration

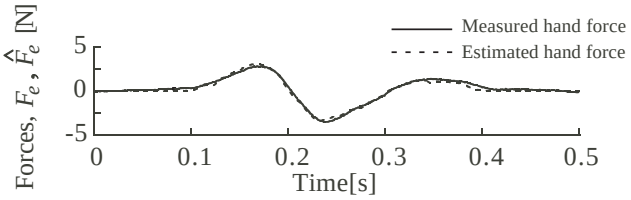

(d) Measured and estimated hand force

Fig. 11. An example of measured signals for task-readiness impedance measurement (Subject C)

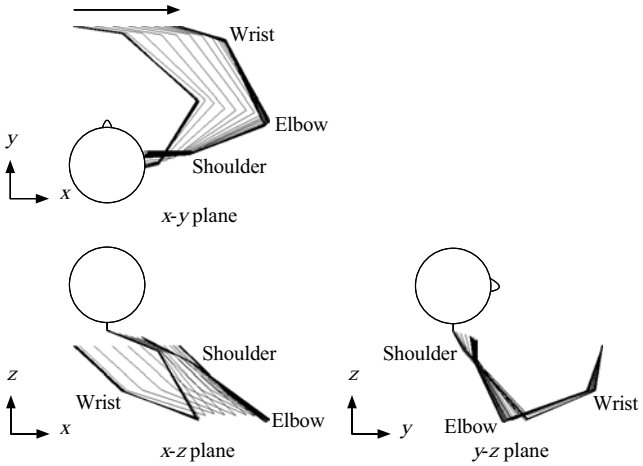

(a) Unskilled subject A

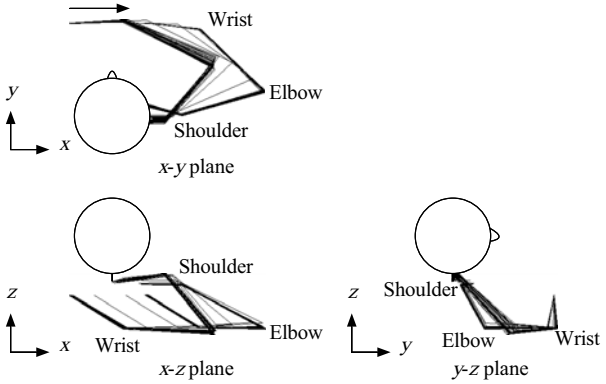

(b) Skilled subject C

Fig. 12. An example of measured arm postures during the ball-catching task

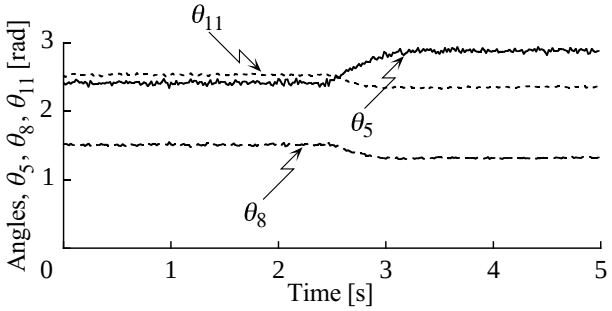

(a) Unskilled subject A

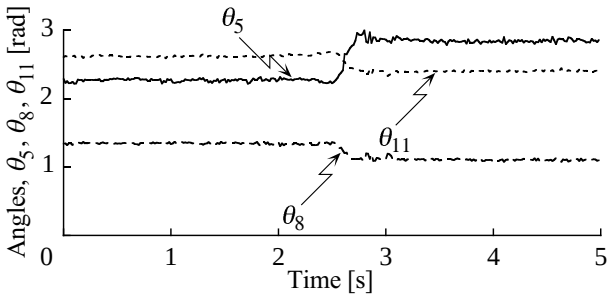

(b) Skilled subject C

Fig. 13. An example of measured joint angles during the ball-catching task

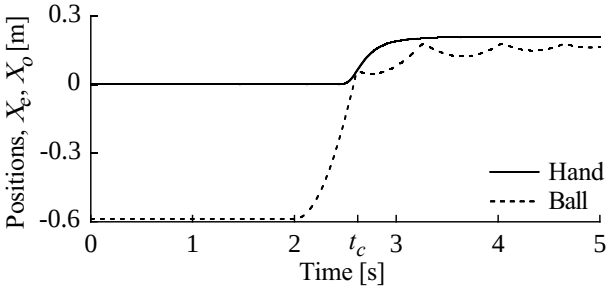

(a) Hand and ball positions

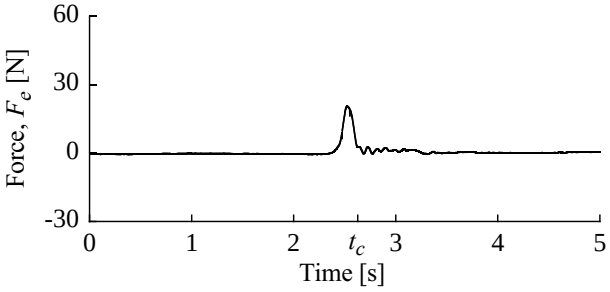

(b) Hand force

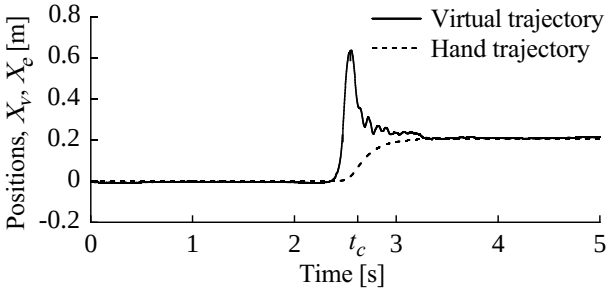

(c) Hand position and virtual trajectory

Fig. 14. Estimated virtual trajectory of the unskilled subject A under $B_r = 20$ [Ns/m]

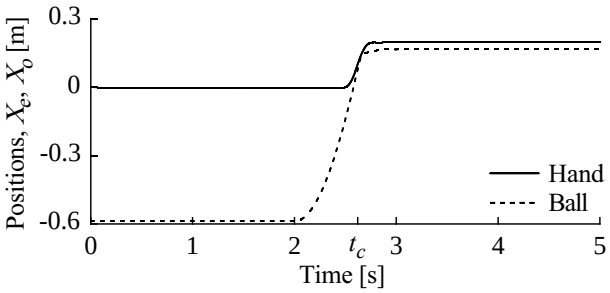

(a) Hand and ball positions

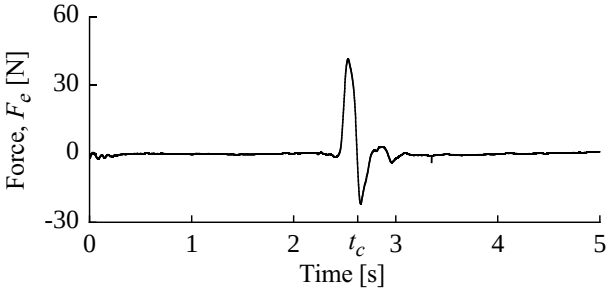

(b) Hand force

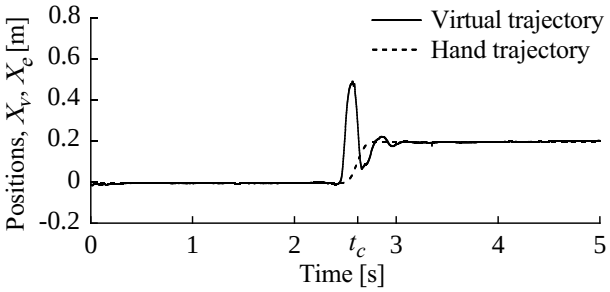

(c) Hand position and virtual trajectory

Fig. 15. Estimated virtual trajectory of the skilled subject C under $B_r = 20$ [Ns/m]

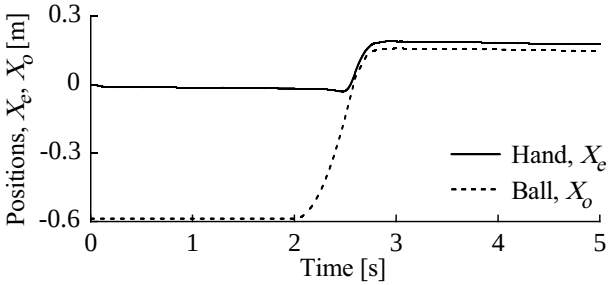

(a) Subject C ($F_{int}^{max} = 17.81$ [N], $t_{int} = 2.05$ [s])

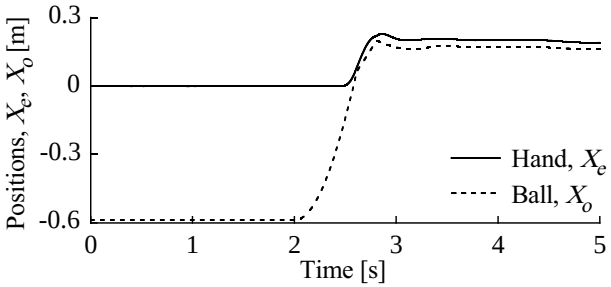

(b) Subject D ($F_{int}^{max} = 22.45$ [N], $t_{int} = 1.55$ [s])

Fig. 16. An example of experimental results of the subjects for $B_r = 5$ [Ns/m]

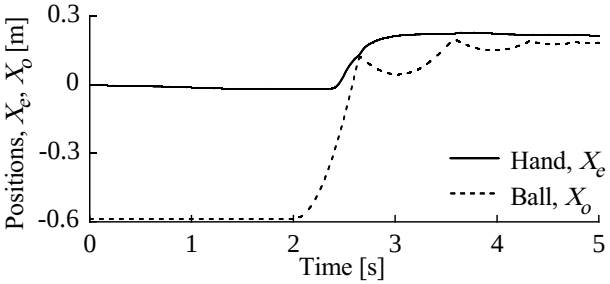

(a) Simulated hand and ball positions

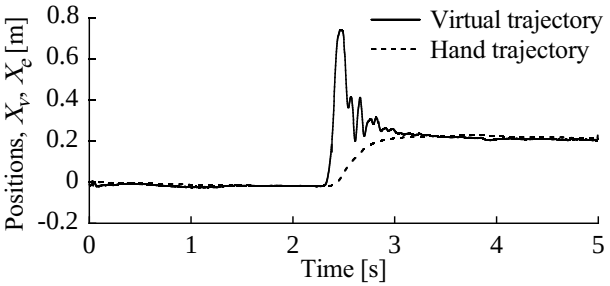

(b) Estimated virtual trajectory

Fig. 17. Simulation results with the task-readiness impedance of the unskilled subject (Subject A) under $B_r = 20$ [Ns/m]

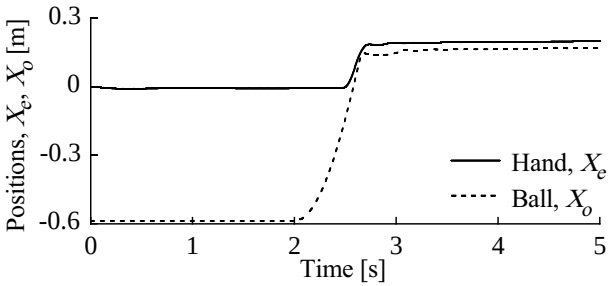

(a) Simulated hand and ball positions

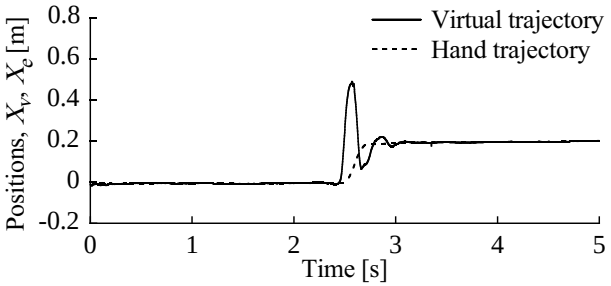

(b) Estimated virtual trajectory

Fig. 18. Simulation results with the task-readiness impedance of the skilled subject (Subject C) under $B_r = 20$ [Ns/m]